STATISTICS, OPTIMIZATION AND INFORMATION COMPUTING
Stat., Optim. Inf. Comput., Vol. **16**, August 2026, pp 1394–1416.
Published online in International Academic Press (www.IAPress.org)

Biomimetic Design of a Brown Bear Claw-Inspired Subsoiling Shank: Design, DEM Simulation, and Field Validation

Ahmed M. Hassan [1,2], Abouelnadar El Salem [1,3,*], Reham M. Kamel [4], Xiaoshuai Zheng [5,6], Fatma A. Atia [7], Sayed Youssef [8], Fatma M. Shaaban [2]

[1] *School of Life Science and Food Engineering, Huai'an University, Huai'an, 223003, China*
[2] *Agricultural Engineering Department, Faculty of Agriculture, Ain Shams University, Cairo 11241, Egypt*
[3] *Soil Conservation Department, Desert Research Center, Cairo 11753, Egypt*
[4] *Agricultural Engineering Research Institute, Agricultural Research Center, Giza 12611, Egypt*
[5] *Yellow River Delta Intelligent Agricultural Machinery Equipment Industry Academy, Dongying 257300, China*
[6] *Qingdao University of Technology, Qingdao 266520, China*
[7] *College of Business, Imam Mohammad Ibn Saud Islamic University (IMSIU), Riyadh 11432, Riyadh, Saudi Arabia*
[8] *College of Languages and Translation, Imam Mohammad Ibn Saud Islamic University (IMSIU), Riyadh 11432, Riyadh, Saudi Arabia*

Abstract Subsoiling is essential for alleviating soil compaction, improving water infiltration, and enhancing soil structure; however, conventional tools often require high draft force and produce inefficient soil disturbance. Inspired by the penetration mechanism of brown bear claws, this study proposes a biomimetic subsoiling shank to improve soil-cutting efficiency and disturbance quality. A discrete element method (DEM) model was developed using a linear cohesion-integrated hysteretic spring contact model to simulate soil–tool interaction. Model parameters for loam soil from the Yellow River Delta (China) were calibrated using angle of repose tests, direct shear tests, and bulk density matching. Validation against experimental data showed good agreement, with a draft force error of $\sim$10%. While the DEM model demonstrated good accuracy for draft force prediction, the simulation of soil disturbance geometry was moderately accurate, with relative errors ranging from 16.6% to 32.8%. Soil disturbance profiles were quantified using gradient-based image processing in MATLAB and geometric reconstruction in AutoCAD. Field experiments were conducted to validate the DEM model and measure the absolute performance of the bioinspired shank; owing to unavoidable variation in operating conditions between tools, the controlled DEM model was used for the formal comparative analysis. Comparative DEM simulation results indicated that the biomimetic shank reduced draft force by 6.1%, increased furrow cross-sectional area by 8.6%, and decreased ridge height by 25.6% compared to a conventional design. Parametric analysis confirmed that rake angle and tillage depth significantly affect performance. The improved efficiency is attributed to optimized stress distribution and soil flow induced by the claw-inspired geometry. The findings demonstrate the potential of biomimetic design and the effectiveness of the validated DEM model for optimizing soil-engaging tools.

Keywords Biomimetics, bioinspired subsoiler; brown bear claw, bionic; draft force; soil disturbance; DEM.

DOI: 10.19139/soic-2310-5070-4221

1. Introduction

Subsoiling has become an essential tillage practice for alleviating soil compaction, reclaiming salt-affected soils, enhancing soil chemical and physical properties, and thereby improving crop growth and yield parameters [1, 2]. However, despite these well-documented benefits, subsoiling operations require significantly higher draft forces and consume much more energy—typically three to five times that of harvesting tools and seeders [3]. This excessive energy demand arises from several interrelated factors: the deeper tillage depths required to fracture

*Correspondence to: Abouelnadar El Salem (Email: salem@yrdia.cn; Tel.: +86 15554645849). School of Life Science and Food Engineering, Huai'an University, Huai'an, 223003, China.

ISSN 2310-5070 (online) ISSN 2311-004X (print)
Copyright © 2026 International Academic Press

compacted subsoil layers, the soil's adhesive nature, which increases friction against tool surfaces, and the considerable mechanical work required to disrupt dense soil structures [4]. The significant power requirements of subsoiling, coupled with rising energy costs, require innovative design strategies that maintain or improve soil loosening quality while reducing draft forces.

Sun et al. [4] designed bionic subsoilers inspired by the drag-reducing riblet structures found in shark skin. Their discrete element method (DEM) simulations demonstrated that subsoilers featuring bionic triangular prism elements arranged horizontally along the direction of motion reduced draft force requirements by up to 21.9% and total energy consumption by 24.8% compared to conventional subsoilers. Additionally, these designs exhibited enhanced soil disturbance characteristics, such as increased soil porosity and reduced soil swelling. Similarly, Wang et al. [3] developed a cicada-inspired subsoiling tool that mimicked both the head shape and movement of the cicada. This innovative design led to reductions in draft force of up to 17.7% across various working depths and speeds. The cicada-inspired tool not only decreased draft forces but also improved soil surface flatness and increased soil loosening efficiency by up to 17.37% compared to traditional chisel subsoilers. In addition to geometric modifications, Barzegar et al. [5] explored material-based strategies by coating furrowers with ultra-high-molecular-weight polyethylene (UHMW-PE). Soil bin tests conducted in heavy clay indicated that this surface modification could reduce draft force by 29% to 54%, depending on moisture content and compaction levels, while eliminating the soil adhesion issues faced by conventional steel tines. These studies underscore how innovative design strategies can effectively address the trade-offs between draft force reduction and soil loosening quality.

The assessment of tillage forces and soil disturbance is critical for evaluating the performance of soil-engaging tools. Recent research has increasingly utilized the discrete element method (DEM) as a sophisticated numerical method for simulating soil-tool interactions by modeling individual particle contacts. Li et al. [6] developed a DEM model in PFC^{3}D to simulate the interaction between a bear claw and soil, calibrating critical model parameters, such as particle stiffness, by comparing simulated cutting forces and soil disturbance width with predictions from the universal earthmoving equation. Their validated model successfully examined the effects of rake angle and working depth on soil disturbance characteristics, including changes in soil porosity and the number of particles dislodged. Similarly, Hang et al. [7] employed EDEM software to investigate the effect of tine spacing on soil disturbance during subsoiling, using a Hertz-Mindlin model with bonding contacts to simulate the cohesive behavior of a loamy clay soil. They monitored soil particle forces and velocities at different depths, and validated their simulations against field experiments by comparing soil disturbance profiles, undisturbed soil height, and soil looseness. In a related approach, Aikins et al. [8] calibrated the input parameters for a DEM model focused on a highly cohesive Black Vertosol soil. They employed a hysteretic spring contact model paired with a linear cohesion model and introduced a novel particle displacement analysis to more accurately predict the boundaries of loosened furrows. Their validated DEM model effectively predicted furrow parameters, including cross-sectional area, furrow width, and critical depth, with relative errors typically ranging from 1% to 19%. Using the same contact model, Ucgul and Saunders [9] successfully simulated the interaction between soil and mouldboard ploughs. Their results achieved accurate predictions of draft forces, with discrepancies of 1.9%–16.6% relative to measured values, and of furrow profile areas, with errors of 0.8%–16.5%, across different operating depths, speeds, and implement widths. Collectively, these studies demonstrate that the discrete element method, when rigorously calibrated, is an effective numerical tool for evaluating tillage forces and soil disturbance patterns.

The rake angle of a soil-engaging tool is a crucial design parameter that significantly affects both the mechanical resistance encountered during tillage and the quality of soil disturbance. Extensive research has focused on understanding this relationship, revealing a complex interaction that depends heavily on the tool's geometry and soil conditions. McKyes and Maswaure [10] demonstrated that while the cross-sectional area of disturbed soil did not change significantly with rake angle (varying by less than 12% across angles from 30° to 90°), the draft force increased considerably, more than doubling from 3.55 kN at a 30° rake angle to 7.26 kN at 90°. More recent investigations using advanced discrete element method (DEM) simulations have provided deeper insights into these mechanistic effects. For example, Barr et al. [11] showed that rake angle openers ranging from 35° to 53° encourage the vertical movement of deeper soil upwards along the furrow profile, thereby enhancing the mixing of soil layers. In contrast, steeper rake angles (between 72° and 90°) tend to throw soil laterally, resulting in greater soil disturbance. In a similar context, Hoseinian et al. [12] reported that increasing the share rake angle from 7.5° to

40° enhanced soil pulverization, while the cross-sectional area of disturbed soil remained largely unaffected. They attributed the observed 17.4% increase in specific resistance (SR) to this enhanced soil pulverization.

The objectives of this study were to: (1) design and evaluate a bear claw-inspired subsoiling shank inspired by the brown bear's exceptional digging abilities in challenging soil conditions; (2) determine adequate DEM input parameters for loam soil in the reclamation region of the Yellow River Delta (YRD), China; and (3) investigate the effects of cutting share rake angle and tillage depth on the performance of the bioinspired subsoiler.

2. Methodology

2.1. Quantification of the Bionic Prototype Morphology

The brown bear (*Ursus arctos*) possesses strong, gently curved claws measuring between two and four inches in length. This physical adaptation is particularly well-suited for digging roots and creating dens in compacted soil. Based on this effective digging ability, the current study used the edge contours of the bear's middle claw as a model to design a new bioinspired chisel shank. To analyze claw morphology, a precise image-based quantification method was developed using MATLAB's Image Processing Toolbox. This method included a scaling procedure to ensure dimensional accuracy in the real world. The workflow began by marking two reference points (a_1 and a_2) on the lateral profile of the claw. Next, the actual distance between these points (D_a) was measured using a digital vernier caliper (Model 01407A, NEIKO Tools USA, USA) with a measuring range of 0–150 mm, a resolution of 0.01 mm, and an accuracy of ±0.02 mm. An image was then captured perpendicularly to the plane containing the lateral profile, which helped minimize perspective distortion. The image was imported into MATLAB, where the distance between the two marked points was measured in pixels (D_p). Finally, a scaling factor ($S = D_a/D_p$) was calculated to convert the pixel dimensions into real-world units.

The image was converted to grayscale and then binarized. After that, morphological operations, such as dilation and erosion, were applied to improve the binary mask. Hole filling was used to remove internal artifacts, and the Canny edge detector was utilized to extract the outer boundaries of the claw. The Canny edge detector was selected for its multi-stage algorithm, which includes Gaussian filtering for noise reduction, gradient calculation for edge strength and direction, non-maximum suppression for edge thinning, and hysteresis thresholding for distinguishing genuine edges from noise. Its accuracy, precise localization, and noise minimization made it well-suited for reliable quantification in this biomimetic design application. The bionic prototype was defined by two primary contours: an inner edge outlining the soil-engaging surface and an outer edge corresponding to the dorsal profile (Figure 1). In practical applications, the claw engages with the soil only below the c-point [6]. Accordingly, following edge detection, the contours were digitized solely up to this point, and polynomial curve fitting was subsequently applied to the resulting profiles, achieving a coefficient of determination (R^2) greater than 0.995 to ensure high-fidelity representation. The fitted curve was then scaled proportionally to achieve a shank length of 350 mm and extended laterally to an overall width of 25 mm, generating the final geometry of the bioinspired curved chisel shank.

2.2. Determination of Soil Physical and Mechanical Properties

The physical and mechanical properties of the soil were characterized according to standard laboratory procedures. Gravimetric moisture content was determined by oven-drying field-moist samples at 105°C for 24 hours until a constant mass was achieved, with water loss calculated relative to the final dry mass, yielding a moisture content of 19.6%. Wet bulk density was measured using the core method, in which undisturbed samples were collected in stainless steel cylinders (61.8 mm diameter, 20 mm height), and the wet mass was divided by the core volume, yielding a wet bulk density of 1516 kg·m^{-3}. Particle size distribution was determined using laser diffraction (Mastersizer 3000+, Malvern Panalytical, UK), enabling classification of the soil texture based on the percentages of sand, silt, and clay. The analysis yielded a sand fraction of 48.1%, a silt fraction of 35.2%, and a clay fraction of 16.7%. According to the USDA textural triangle, these values classify the soil as loam.

The liquid limit and plastic limit of the soil were determined according to the procedures outlined in ASTM D4318 and ISO/TS 17892-12. The liquid limit was measured using the Casagrande cup method, while the plastic

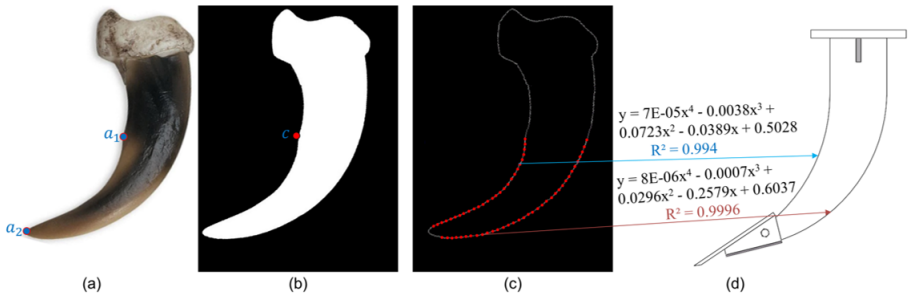

Figure 1. Development of the bio-inspired curved chisel shank: (a) RGB image of the bionic prototype; (b) extracted lateral profile of the bionic prototype; (c) digitized contours outlining the outer boundaries of the claw; (d) final geometry of the chisel shank generated from the scaled and extended fitted curve.

limit was assessed by repeatedly rolling a soil sample by hand on a glass plate until threads began to crumble. The tests yielded a liquid limit of 31% and a plastic limit of 19%. Soil penetration resistance was measured in undisturbed soil using a digital cone penetrometer equipped with a standard 30° apex angle cone (12.83 mm diameter). The penetrometer was inserted vertically to a depth of 250 mm, yielding a penetration resistance of 2.11 MPa. Soil salinity was assessed by measuring the electrical conductivity of the centrifuged solution, yielding an EC of 2.79 dS·m^{-1} for the soil extract at field moisture content (19.6%).

2.3. DEM-modeling Setup for Subsoiling

To accurately capture both interparticle interactions and the interactions between particles and tools within the reclamation area of the Yellow River Delta (YRD), a linear cohesion-integrated hysteretic spring contact model was adopted to simulate the cohesive-frictional behavior of the soil [11, 14, 13]. The calibration of the discrete element model (DEM) and the contact model parameters was performed through multiple experimental and iterative simulation steps.

2.3.1. Determination of Interparticle Interaction Parameters The angle of repose test is a well-established method for evaluating the flowability and interparticle friction of granular materials, including soils [15]. In this study, the coefficients of static and rolling friction between particles were calibrated using the angle-of-repose test, following the methodology presented by Aikins et al. [8]. The lifting cylinder method was employed, using a cylindrical pipe with an inner diameter of 90 mm and a height of 250 mm. This pipe was filled to a depth of 150 mm with loose soil at a moisture content of 19.6%. The cylinder was then raised vertically at a constant rate of 36.7 mm/s until it cleared the soil, allowing the material to form a pile. The resulting soil mound was collected in a cap (100 mm inner diameter, 28 mm deep) placed beneath the pipe, and the test was conducted in triplicate.

Due to the poor flowability of the tested soil, the accumulated material formed a dome-shaped pile rather than a conical pile, making it impossible to measure a definitive angle of repose. As a result, the height of the formed pile was used as the comparative metric for comparing experimental measurements with discrete element method (DEM) simulations. In the DEM simulation, the experimental procedure was replicated, and the interparticle static and rolling friction coefficients were adjusted iteratively until the simulated pile height closely matched the experimental value. This approach yielded good agreement, with static and rolling friction coefficients of 0.6 and 0.29, respectively, resulting in a simulated pile height of 53 mm that closely matched the experimentally measured mean height of 55 mm (Figure 2).

2.3.2. Determination of Soil–Tool Interaction Parameters The soil-steel static coefficient of friction was measured using the inclined-plane test, in accordance with ASTM G219. In this method, a soil specimen was placed on a rectangular steel plate (40 cm length, 7.5 cm width), representing the tool material. The inclined plane was then raised at a controlled rate of 7 mm min^{-1}. This rate was chosen to maintain quasi-static conditions, ensuring

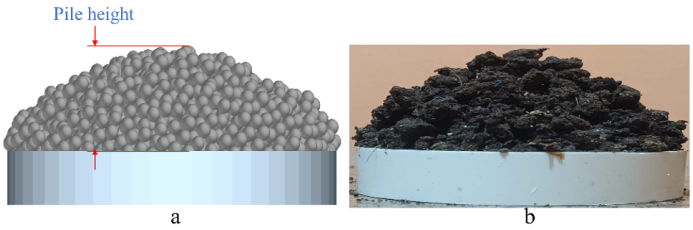

Figure 2. Soil pile created during the angle of repose test using the lifting cylinder method: (a) DEM-simulated pile and (b) experimental pile.

that inertial effects did not affect the measured friction angle until the soil specimen began to slide. The static coefficient of friction was calculated as the tangent of the angle at which sliding started. The soil-steel rolling friction coefficient was sourced from Aikins et al. [8], who reported a value of 0.216 for a Black Vertosol under comparable conditions. Additionally, the soil-steel coefficient of restitution was set at 0.3, based on the value used by Hang et al. [7].

2.3.3. Contact Models Input Parameters Calibration The input parameters for the hysteretic spring contact model include the damping factor, the stiffness factor, the soil's yield strength, and the tool material's yield strength. In contrast, the linear cohesion model requires two additional parameters: interparticle cohesive energy density and soil-tool adhesive energy density. The damping factor and stiffness factor for both soil particles and the tool material were set to 0.05 and 0.95, respectively [16]. Soil-steel adhesion was measured using a strain-controlled direct shear box apparatus (ZJ Model, Nanjing Soil Instrument Factory Co., Ltd., China). A cylindrical steel block (62 mm diameter, 12 mm height) was placed in the upper (movable) half of the shear box, while the lower (fixed) half was filled with remoulded soil. The soil sample was prepared by breaking down, sieving, hydrating the material to a moisture content of 19.6%, and compacting to a bulk density of 1516 kg·m^{-3}. A constant shear rate of 2 mm min^{-1} was applied throughout the test. Normal loads of 15, 25, 35, and 45 kPa were applied. The direct shear tests yielded an adhesion value of 11,489 J·m^{-3}, determined from the y-axis intercept of the failure envelope using the Mohr-Coulomb failure criterion (Figure 3).

Using the experimentally measured soil wet bulk density as the target for simulating particle packing is an effective approach for modeling soil-tool interactions in sticky soil conditions [14]. El Salem et al. [13] demonstrated that key parameters influencing packing density in DEM simulations include particle yield strength, interparticle cohesive energy density, and the interparticle coefficient of restitution. As a result, these parameters were calibrated using the soil's experimentally measured wet bulk density as the target. A central composite design was employed to determine the parameter set that minimizes the discrepancy between the simulated particle packing density and the soil experimentally measured bulk density.

The calibration ranges for each parameter were established based on the findings of El Salem et al. [13]. The experimental design was generated and analyzed using Design-Expert software, with five replications at the center point. A face-centered Central Composite Design (CCD) was chosen because a preliminary analysis revealed that particle packing density is highly sensitive to particle yield strength at low parameter values. By setting the axial distance $\alpha = 1$, this design confines all experimental points within the original factor space, ensuring that the response is evaluated solely within the predefined region of interest.

2.4. DEM Model Setup for Subsoiling Simulation

To create the soil model, spherical particles with a normally distributed diameter ranging from 7.6 to 8.4 mm were generated using a static particle factory within a virtual soil bin measuring 2000 mm × 800 mm × 900 mm. The 800 mm width was chosen to provide adequate space for lateral soil displacement during tool advancement. The 2000 mm length ensured the subsoiler reached a steady-state operating condition and provided an appropriate measurement zone for reliable data acquisition. The fill section option was used to randomly assign the particles'

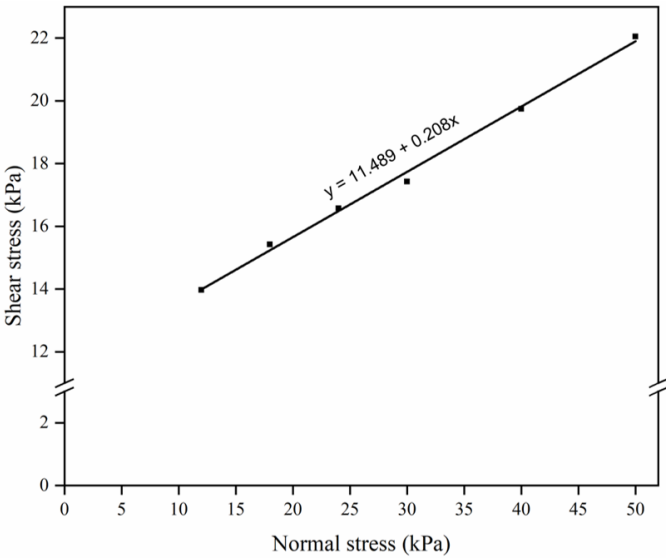

Figure 3. Direct shear test results for the soil–steel interface.

initial positions and orientations. After their generation, the particles were allowed to settle under a constant gravitational acceleration of 9.81 m/s^2 in the vertical (Z) direction. After 3 seconds, determined to be sufficient for stabilization, which is defined as the point at which the total number of interparticle contacts ceased to increase, the effective depth of the soil domain was reduced to 250 mm by removing particles above the target surface elevation. CAD models of both the bioinspired and conventional shanks were developed in SolidWorks 2020 and then imported into EDEM 2020.0 to perform discrete element method (DEM) simulations. The geometries of both shanks are presented in Figure 4.

2.5. Assessment of Soil Disturbance

To quantitatively characterize the DEM-simulated profiles of the loosened areas, it is essential to establish appropriate thresholds based on criteria such as particle count, velocity, or displacement. Several methodologies have been discussed in the literature for this purpose. Hang et al. [7] defined disturbed particles as those with non-zero velocities. Meanwhile, Murray [17] set a threshold of 5 mm for resultant displacement to differentiate the loosened zone from the undisturbed furrow boundary.

In the current study, the three-dimensional lattice grid implemented in EDEM was used to count particles within discrete volumetric cells. This approach allows for the identification of the boundary between loosened and undisturbed particles. The key principle is that grid cells containing loosened particles have lower particle counts compared to those in undisturbed regions. The size of the grid cells is critical for minimizing truncation errors and ensuring an accurate definition and representation of the loosened particle boundary [11]. Accordingly, grid cells with a width and height equivalent to 2.4 times the nominal particle radius and a length of 600 mm were adopted in this study, following the recommendation of Aikins et al. [8]. Particle count data within the grid cells were visualized as a heat map, with each pixel's brightness indicating the number of particles (Figure 5). To objectively determine the boundary between loosened and undisturbed soil regions, the gradient magnitude of the heat map image was calculated using MATLAB's imgradient function. A threshold was subsequently applied to the gradient magnitude to extract the furrow profile, defined as the contour corresponding to significant local changes in particle density. The threshold value was selected iteratively by comparing the extracted boundary against the experimentally measured furrow profile (Figure 10) and choosing the value that minimized the cumulative boundary deviation. A sensitivity analysis confirmed that varying the threshold by ±15% around the selected value produced changes of less than 5% in the computed furrow cross-sectional area, indicating that the results are not

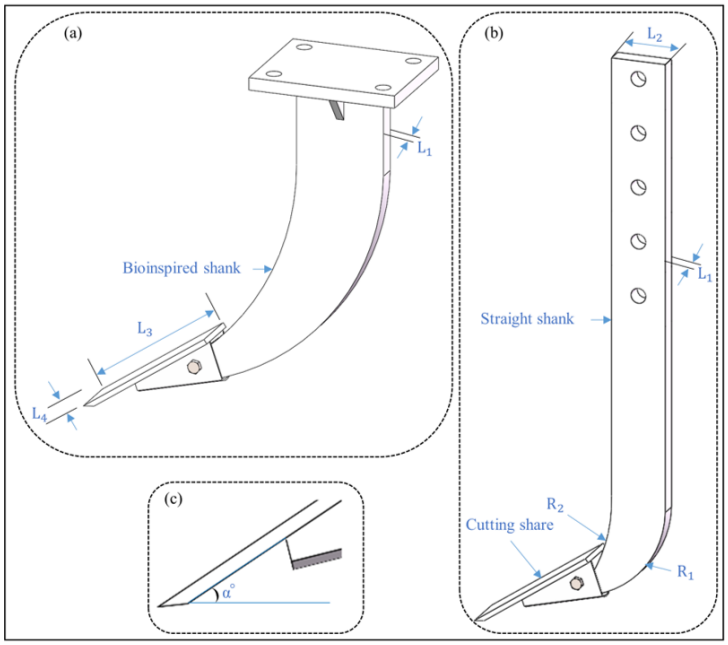

Figure 4. Geometric configurations of the subsoiling tools used in this study: (a) bioinspired subsoiling tool featuring biomimetic curves; (b) conventional straight chisel subsoiling tool; and (c) definition of the plowing rake angle (α). Geometric parameters: $L_1 = 25$ mm, $L_2 = 80$ mm, $L_3 = 165$ mm, $L_4 = 40$ mm, $\alpha = 35^\circ$ (rake angle), $R_1 = 145$ mm, $R_2 = 230$ mm.

highly sensitive to the precise threshold choice. Moreover, the quantity of dislodged particles, defined as the count of soil particles scattered above the original undisturbed surface following tillage, served as a metric for assessing the lifting action of both chisel shanks.

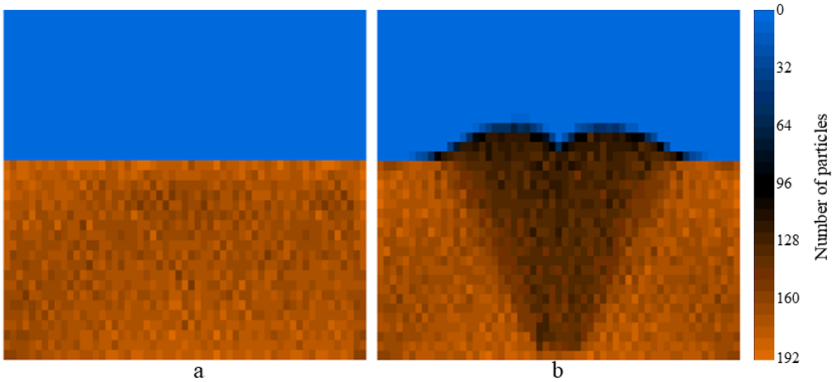

Figure 5. Particle distribution within the lattice grid monitoring zone in EDEM: (a) Initial state before tillage, showing the baseline soil particle distribution; and (b) Final state after tillage, illustrating the soil disturbance caused by shank interaction. The heatmap is best interpreted in color; a color bar is recommended.

2.6. Integrated performance index

An integrated performance index was developed using multiple tillage effectiveness indicators to evaluate the bioinspired subsoiler across different rake angles. The primary focus was on reducing draft force, as it is directly linked to lower energy consumption. Moreover, the minimal ridge height was considered beneficial for creating a smoother soil surface, while increased lateral soil throw was considered advantageous for better residue incorporation. This incorporation is important because soil placed over crop residues accelerates decomposition and improves subsequent soil properties. Additionally, targeting a greater reduction in post-tillage bulk density was essential to achieve the main goal of loosening the soil. Therefore, superior tool performance was characterized by lower draft force, reduced ridge height, increased lateral soil throw, and enhanced porosity.

$$I = \frac{\phi \times S_{lt}}{F_d \times R_h} \tag{1}$$

where I is the performance index, ϕ is the post-tillage bulk density reduction (%), S_{lt} is the lateral soil throw (mm), F_d is the draft force (N), and R_h is the ridge height (mm).

McKyes and Maswaure [10] defined soil loosening efficiency as the disturbed cross-sectional area per unit of draft. In the present study, a specific loosening resistance, defined as the draft force per unit reduction in post-tillage bulk density, was used to describe the bioinspired subsoiler's performance at varying tillage depths. This approach assumes that the reduction in post-tillage bulk density within the designated analysis zone is positively correlated with the disturbed cross-sectional area.

2.7. Field Experiments

Chiseling experiments were conducted using the bioinspired subsoiler in a field located within the reclamation region of the Yellow River Delta (YRD) in Dongying City, China (118° 39 9 E, 37° 18 39 N). A 150-horsepower tractor (John Deere model 6E-1504-PL) equipped with a standard three-point hitch was used to operate the chisel shank (Figure 6). The draft force of the shank was measured using three S-shaped load cells (model SBT620TF; capacity: 1000 kg), and the total net draft force (F_d) in the direction of travel was calculated in real time by summing the horizontal force components from each sensor. During each pass, draft force data were continuously recorded using a multi-channel dynamic signal acquisition system (DH3820 N Distributed Stress-Strain Test and Analysis System, Donghua Testing Technology Co., China). Following each pass, the average tillage depth was determined by excavating the loosened soil and measuring the depth to the undisturbed soil surface. Operating speed was calculated by timing the tractor over a fixed 50 m travel distance within the test plot. The experiment was conducted with five replicates. Five replicates were deemed sufficient given the primary purpose of the field test: validation of the DEM model, rather than definitive inter-tool comparison, and are consistent with similar DEM validation studies in the tillage literature [8, 9]. The operating speed of 1.34 ± 0.05 m·s^{-1} measured during field validation was consistently applied as the fixed speed in all subsequent DEM parametric studies (Sections 3.5.1–3.5.5) to ensure comparability between simulation and field conditions. The resulting mean draft force, tillage depth, and operating speed were 927 ± 45 N, 224 ± 18 mm, and 1.34 ± 0.05 m·s^{-1}, respectively.

2.7.1. Quantification of Furrow Profiles from Field Experiments Furrow profiles were quantified by scanning the resulting top-surface profile after tillage with a soil profiler (100 cm wide and 30 cm high). The apparatus consisted of 120 steel pins arranged in a contiguous array. Following this initial scan, the loosened soil was carefully excavated, and a second scan was conducted to capture the furrow failure boundary (Figure 7a) [7]. For each chisel shank, four measurement locations were randomly selected, with a separation distance of 10 m to ensure spatial independence. All test points were positioned away from both the start of the work stroke and the field boundaries to avoid edge effects and to ensure steady-state operating conditions. To evaluate soil disturbance, several parameters were extracted from the resulting furrow profiles, namely: furrow cross-sectional area, furrow width, lateral soil throw, and ridge height (Figure 7b). The cross-sectional areas of the created furrow profiles were quantified using AutoCAD software [4]. First, the BOUNDARY command was employed to generate a closed polyline around each region of interest. In the Boundary Creation dialog box, the object type was set to "Polyline" with island detection enabled. An internal point was then selected within the target zone, and AutoCAD automatically generated a closed

Figure 6. Measurement of draft force for the bioinspired subsoiler: (a) experimental setup; (b) soil-tool adhesion phenomena of the wet soil; (c) resulting furrow profile.

polyline coincident with the surrounding curves. Following boundary creation, the area of the selected object was obtained using the LIST command.

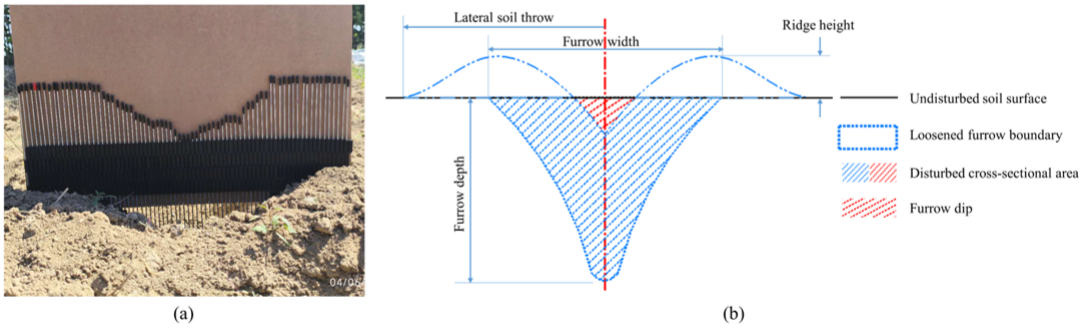

Figure 7. Quantification of the experimentally obtained profile curve: (a) post-excavation scan showing the furrow failure boundary after removal of the loosened soil; (b) schematic representation of the disturbed soil boundary with the corresponding evaluation parameters.

3. Results and Discussion

3.1. Model Calibration

The full design matrix and simulation results from the face-centered Central Composite Design are presented in Table 1. The statistical significance of the full quadratic model terms was assessed using analysis of variance (ANOVA), with the results summarized in Table 2. To simplify the model while maintaining its predictive capability, insignificant terms were removed, yielding the refined quadratic polynomial presented in Equation 2.

$$\rho_b = 2302.433 - 0.027X_1 + 0.019X_2 - 437.43X_3 - 3.2 \times 10^{-7}X_1X_2 + 5.44 \times 10^{-3}X_1X_3 + 2.08 \times 10^{-7}X_1^2 \tag{2}$$

The regression model for the DEM-simulated bulk density was highly significant. The variables X_1, X_2, and X_3, along with the interaction effects X_1X_2 and X_1X_3, as well as the quadratic term X_1^2, all exhibited p-values below 0.01, indicating a statistically significant influence on the DEM-simulated bulk density. The lack-of-fit test

Table 1. Results of the Central Composite Design (CCD) DEM experiment.

Run no.	X_1 **(Pa)**	X_2 **(J·m^{-3})**	X_3	ρ_b **(kg·m^{-3})**
1	30000	6000	0.2	1689.15
2	60000	6000	0.2	1419.03
3	30000	12000	0.2	1746.42
4	60000	12000	0.2	1423.28
5	30000	6000	0.6	1572.57
6	60000	6000	0.6	1371.66
7	30000	12000	0.6	1636.59
8	60000	12000	0.6	1374.73
9	30000	9000	0.4	1664.61
10	60000	9000	0.4	1402.35
11	45000	6000	0.4	1477.19
12	45000	12000	0.4	1494.36
13	45000	9000	0.2	1513.14
14	45000	9000	0.6	1449.95
15	45000	9000	0.4	1485.15
16	45000	9000	0.4	1486.17
17	45000	9000	0.4	1483.52
18	45000	9000	0.4	1479.05
19	45000	9000	0.4	1481.2

Table 2. Analysis of variance for the full quadratic model of the Central Composite test.

Variance Source	**DF**	**Mean Square**	**F-Value**	**p-Value**
Model	9	22768.27	768.86	< 0.0001
X_1	1	1.74×10^5	5868.64	< 0.0001
X_2	1	2125.18	71.76	< 0.0001
X_3	1	14862.57	501.89	< 0.0001
X_1X_2	1	1623.65	54.83	< 0.0001
X_1X_3	1	2128.46	71.88	< 0.0001
X_2X_3	1	3.88	0.131	0.7258
X_1^2	1	6397.92	216.05	< 0.0001
X_2^2	1	1.28	0.0432	0.84
X_3^2	1	34.36	1.16	0.3095
Residual	9	29.61		
Lack of Fit	5	46.55	5.51	0.0616
Pure Error	4	8.45		
Total	18			

yielded a p-value of 0.0618, indicating that the model fits the data adequately at the 95% confidence level (p ¿ 0.05). Although this value is close to the conventional significance threshold, it suggests that the quadratic model effectively captures the underlying relationship between the factors and the response variable. This marginal p-value can be attributed to the very low pure error observed in the center point replicates (runs 15–19), which provided a rigorous assessment of model adequacy. The high experimental precision of these replicates enhances the sensitivity of the lack-of-fit test. Overall, the non-significant lack-of-fit test indicates that the response surface model is adequate for prediction within the defined design space.

The experimentally measured soil wet bulk density of 1,516 kg·m^{-3} was established as the calibration target. The optimization of the refined regression model was conducted within the experimental factor space using

Design-Expert software. This process yielded the following optimal parameter combination: a soil particle yield strength of 46,574 Pa, a cohesive energy density for soil-soil interaction of 11,862 J·m^{-3}, and an interparticle restitution coefficient of 0.208. This optimized parameter set was then applied in a discrete element method (DEM) simulation, yielding a particle packing density of 1,504 kg/m^3, with a relative error of less than 1% compared to the experimental target. A summary of the measured, calibrated, and adopted from previous literature parameter values for the proposed DEM model is presented in Table 3.

Table 3. Summary of material, interaction, and contact model parameters used in the DEM.

Property	**Value**	**Source**
Poisson's ratio of the soil particle	0.4	[7]
Particle density (kg·m^{-3})	2000	[8]
Shear modulus of soil particle (Pa)	1×10^6	[7]
Interparticle restitution coefficient	0.208	Calibrated
Soil-Soil internal friction coefficient	0.6	Calibrated
Soil-Soil rolling friction coefficient	0.29	Calibrated
Nominal diameter of particles (mm)	8	Chosen
Particle size distribution	0.95 - 1.05	[16]
Poisson's ratio of steel	0.3	[8]
The density of steel (kg·m^{-3})	7865	[8]
Shear modulus of steel (Pa)	7.9×10^{10}	[8]
Restitution coefficient of soil-steel	0.3	[7]
Soil-Steel external friction coefficient	0.71	Measured
Soil-Steel rolling friction coefficient	0.216	[8]
Damping factor	0.05	[16]
Stiffness factor	0.95	[16]
Steel Yield strength (Pa)	3.8×10^8	[8]
Soil Particle Yield Strength (Pa)	46574	Calibrated
Cohesive energy density of soil-soil (J·m^{-3})	11862	Calibrated
Adhesive energy density of soil-steel (J·m^{-3})	11489	Measured

3.2. Model Validation

The calibrated DEM model was validated using the experimentally measured draft force for the bioinspired subsoiler and the evaluation parameters of the disturbed soil profile. The simulated draft force of the bioinspired subsoiling tool was measured in the draft force collection zone to ensure steady-state operating conditions (Figure 8). To facilitate a valid comparison, the simulation was conducted at a working depth of 224 mm, an operating speed of 1.34 m/s, and a rake angle of 35°, consistent with the field experiment. A comparison between the draft force measured during field experiments and that simulated using the calibrated DEM model is presented in Figure 9. Both the experimentally measured and DEM-simulated draft forces fluctuated with displacement, though the oscillations were markedly less pronounced in the simulation results. This difference can be attributed to the largely homogeneous nature of the soil profile used in the DEM model, which does not fully capture the field soil's heterogeneity. Nevertheless, the average DEM-simulated force showed good agreement with the mean experimentally measured force: 834 N and 927 N, respectively, corresponding to a relative error of approximately 10%.

A comparison of the experimentally measured and DEM-simulated disturbed soil profiles is presented in Figure 10. The lateral soil throw, furrow width, and ridge height were determined using the coordinates of the particles that formed the top surface of the soil bin after tillage [8]. The furrow cross-sectional area was delineated from the simulated profile and quantified using the methodologies described in Sections 2.5 and 2.8. A quantitative comparison of the soil disturbance evaluation parameters is presented in Table 4. Overall, the soil disturbance parameters showed acceptable agreement, with relative errors of 16.6% for the furrow cross-sectional area, 32.8%

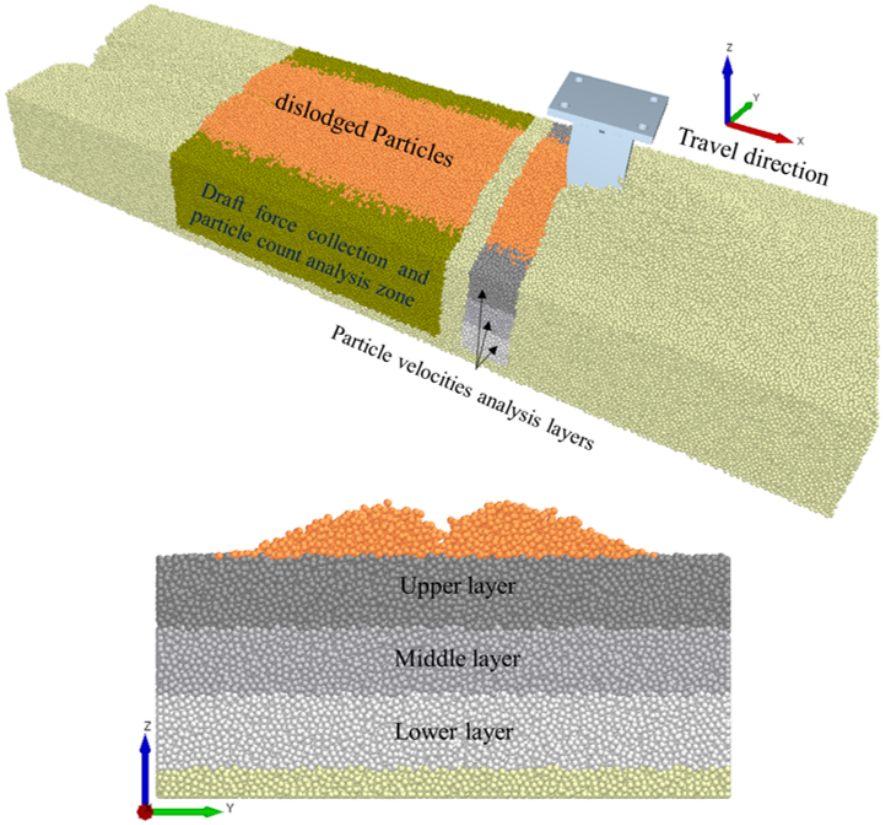

Figure 8. Virtual soil model generated by EDEM, showing the designated analysis zones.

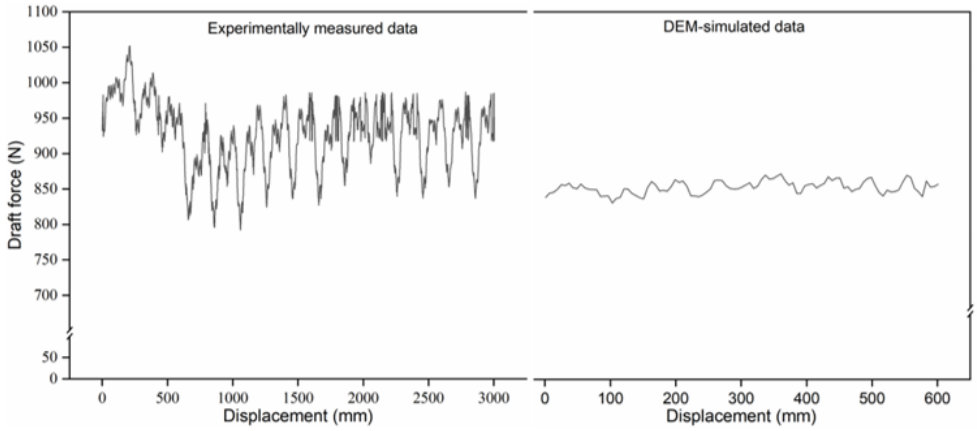

Figure 9. Comparison of the experimental and simulated draft force for the bioinspired subsoiler using the optimally calibrated parameter set.

for the furrow width, 21.7% for the lateral soil throw, and 19.4% for the ridge height. These findings indicate that the proposed model, when properly calibrated using tests such as the angle of repose and direct shear test and factoring in measured soil parameters such as adhesion and wet bulk density, offers a valid approach for predicting both

subsoiling draft force and soil disturbance. Thus, this validated model can serve as a reliable tool for optimizing tillage implements.

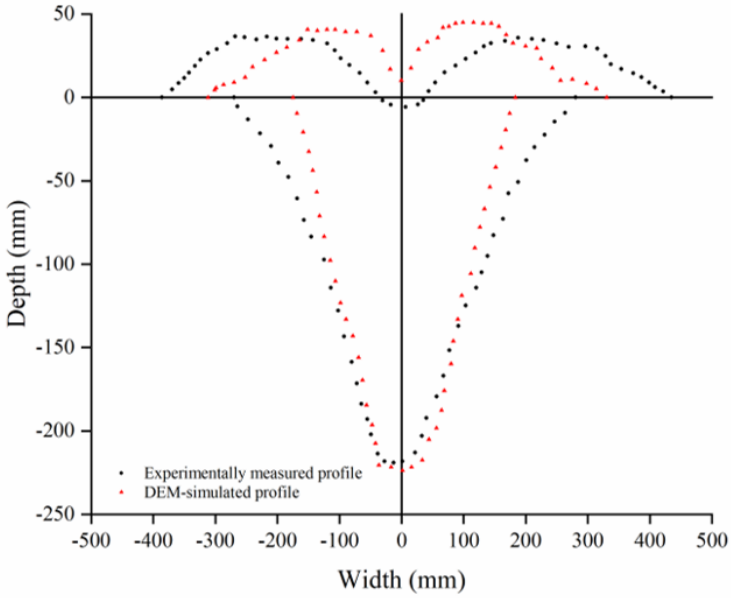

Figure 10. Comparison of experimentally measured and DEM-simulated disturbed soil profiles.

Table 4. Quantitative comparison of measured and simulated soil disturbance parameters.

Parameter	Measured	Simulated	Relative error (%)
Furrow cross-sectional area (mm^2)	65279	54420	16.6
Furrow width (mm)	540	363	32.8
Lateral soil throw (mm)	410	321	21.7
Ridge height (mm)	36	43	-19.4

3.3. Field Experiment Results

The primary purpose of the field experiment described in Section 2.7 was to provide empirical data for validating the DEM model for the bioinspired subsoiler. Both tools were operated at a rake angle of 35°; however, because tractor operating conditions in the field could not be held perfectly constant, the bioinspired subsoiler operated at a mean depth of 224 mm and speed of 1.34 m/s, while the conventional subsoiler operated at 247 mm and 1.26 m/s. Because the operating conditions differed between tools, the field data are reported here as absolute performance metrics and are not used as a direct head-to-head comparison. The formal comparative analysis is presented in Section 3.4, where both tools were evaluated under identical conditions using the validated DEM model. Draft forces measured in the field for both tools are shown in Figure 11 for reference. The bioinspired subsoiler produced a mean draft force of 927 ± 45 N (n = 5), and the conventional subsoiler produced 1092 N under its respective operating conditions. An independent-samples t-test on the bioinspired tool replicates confirmed low inter-replicate variability (CV = 4.9%), supporting the reliability of the DEM validation target. Because the two field datasets were collected under non-identical conditions, no statistical significance test was applied to the inter-tool field comparison; statistical inference on tool performance is based exclusively on the DEM results presented in Section 3.4. The measured draft force for the conventional subsoiler was higher under its respective

(deeper, slower) conditions, which is consistent with the expectation that greater depth increases draft demand. The validated DEM model was therefore used as the controlled, condition-matched environment for evaluating the comparative performance of both subsoilers (Section 3.4).

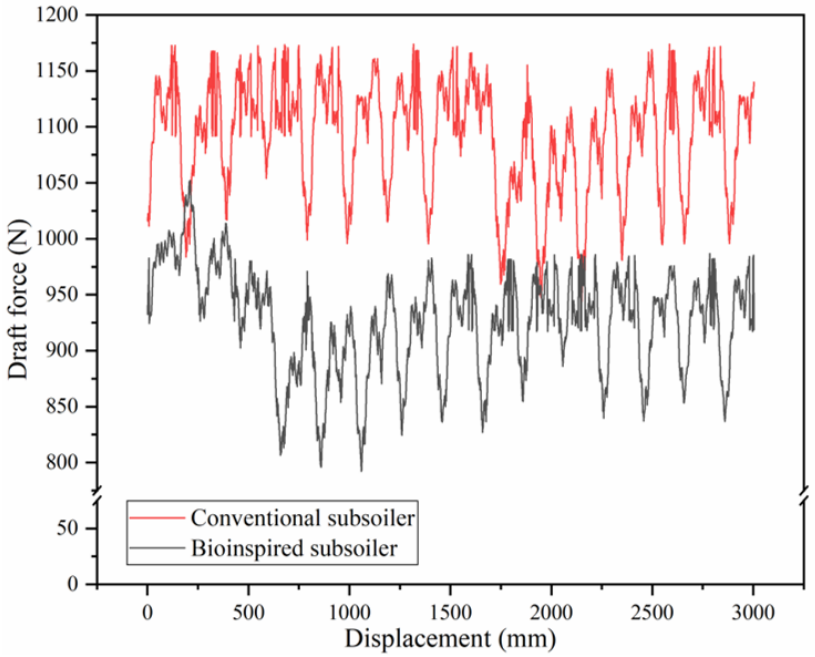

Figure 11. Comparison of the experimentally measured draft forces for the bioinspired subsoiler and the conventional subsoiler.

3.4. Evaluation of the Performance of the Bear Claw-Inspired Subsoiling Tool Using the Validated Model

A comparative study was conducted using the validated model to evaluate the performance of two subsoiling shank designs: a conventional straight shank and a bio-inspired curved shank. To ensure a valid comparison, both shanks were equipped with identical cutting shares measuring 165 mm × 40 mm and operated at the same rake angle of 35° (Figure 4). The evaluation indices included the draft force, soil disturbance evaluation parameters, and the distribution of disturbed soil along the depth profile.

3.4.1. Draft Force A comparison of the DEM-simulated draft force for the bioinspired and conventional subsoiling tools, which operated at a working depth of 224 mm, an operating speed of 1.34 m s^{-1}, and a rake angle of 35°, is presented in Figure 12. For both subsoiler tools, the draft force fluctuates due to the random distribution of soil particles. Peak resistance occurs just before the soil fails, after which the soil particles begin to slip, leading to a temporary decrease in resistance [4]. As the subsoiler continues to move forward, the draft force stabilizes and fluctuates around an average value. The average draft force during this stable fluctuation phase was used for the analysis. The mean draft force for the bioinspired tool was 834 N, compared to 888 N for the conventional tool, representing a relative decrease of approximately 6.1%. Although this reduction is more modest than those reported in previous studies on bioinspired subsoilers, which range from 7.7% to 33.7% depending on the biological prototype and design approach [18, 19, 20], the bioinspired tool demonstrated favorable performance in terms of soil disturbance evaluation parameters and depth-wise distribution of disturbed soil compared to the conventional subsoiler (detailed in Sections 3.4.2 and 3.4.3).

The mechanistic basis for the draft force reduction can be explained through stress redistribution along the shank surface. The curved bear-claw geometry promotes a progressively inclined soil failure plane relative to the direction of travel, which is shorter and less energy-intensive than the near-vertical failure plane formed ahead of the flat-faced conventional shank. Additionally, the curved leading edge distributes the contact stress over a larger surface area, reducing peak normal stress concentrations at the tip and reducing the force required to initiate soil failure (Mohr–Coulomb criterion). In contrast, the straight shank develops a larger passive soil wedge ahead of the tool face, generating higher horizontal resistance. These mechanisms collectively explain the observed 6.1% reduction in draft force for the bioinspired tool.

It should be noted that, while the DEM model was explicitly validated against field data for the bioinspired shank (Section 3.2), an independent field validation was not performed for the conventional shank. The DEM model was applied to the conventional shank using the same calibrated soil parameter set; this is a recognized limitation, and readers should interpret the quantitative inter-tool comparison within this context. The relative performance advantage of the bioinspired shank is considered reliable within the calibrated parameter space. The observed reduction in draft can be attributed to the bear claw-inspired curvature of the cutting edge, which enhances stress dispersion along the edge and more effectively breaks the soil wedge in front of the blade.

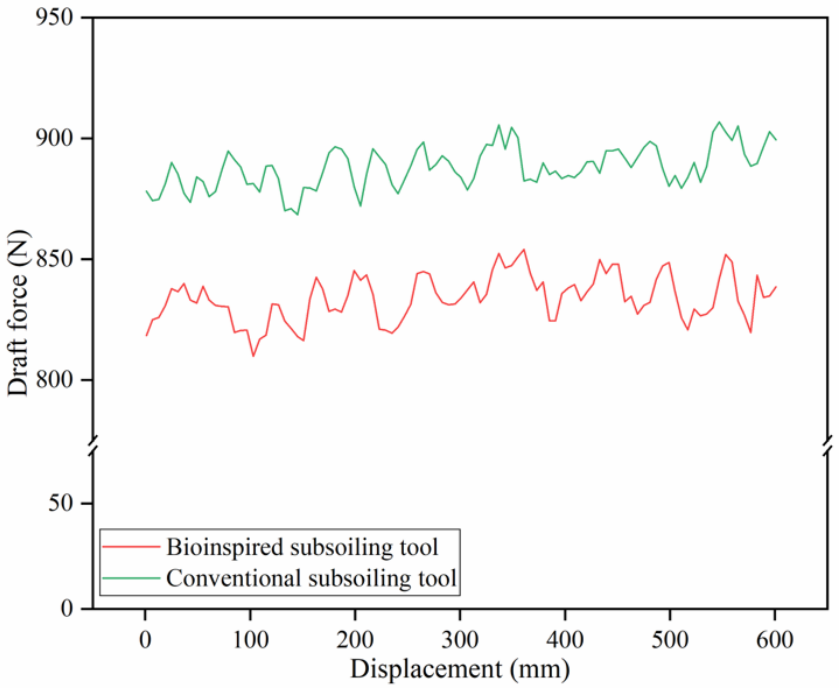

Figure 12. DEM-simulated draft force comparison for the bioinspired and conventional subsoiling tools.

3.4.2. Soil Disturbance Evaluation Parameters The DEM-simulated soil disturbance profiles for both subsoiling tools are displayed in Figure 13. To better quantify soil disturbance, the relevant evaluation parameters derived from these profiles were calculated, and the results are summarized in Table 5. The bioinspired subsoiling tool exhibited better soil disturbance characteristics than the conventional design. The findings indicate that the bioinspired tool creates a larger disturbed soil area, as demonstrated by an 8.6% increase in furrow cross-sectional area and a 7.2% increase in furrow width. Additionally, it results in a smoother soil surface, as shown by a 25.6% reduction in ridge height and a 9.3% increase in lateral soil displacement. The observed improvements in soil disturbance parameters are noteworthy in context: both tools share the same nominal rake angle (35°), so the differences in lateral soil throw and ridge height arise from the curved shank geometry rather than from a change in rake angle

alone. The gradually varying curvature of the bioinspired shank creates a distributed horizontal force component that progressively deflects soil outward along the shank surface; this is mechanistically distinct from the abrupt, concentrated lateral push generated by the straight shank face. Particle trajectory analysis in EDEM confirmed that soil particles in contact with the bioinspired shank follow a more continuous outward arc, whereas particles ahead of the straight shank are predominantly displaced forward before being pushed laterally at the share tip. This distinction is consistent with Section 3.5.4, which shows that reducing the rake angle of a simple flat blade increases lateral throw; the bioinspired curved shank achieves a qualitatively similar effect, enhanced lateral deflection, through geometry-driven flow, not through a lower overall rake angle. may be attributed to the gently curved edge contours of the brown bear claw, which enhance soil loosening efficiency.

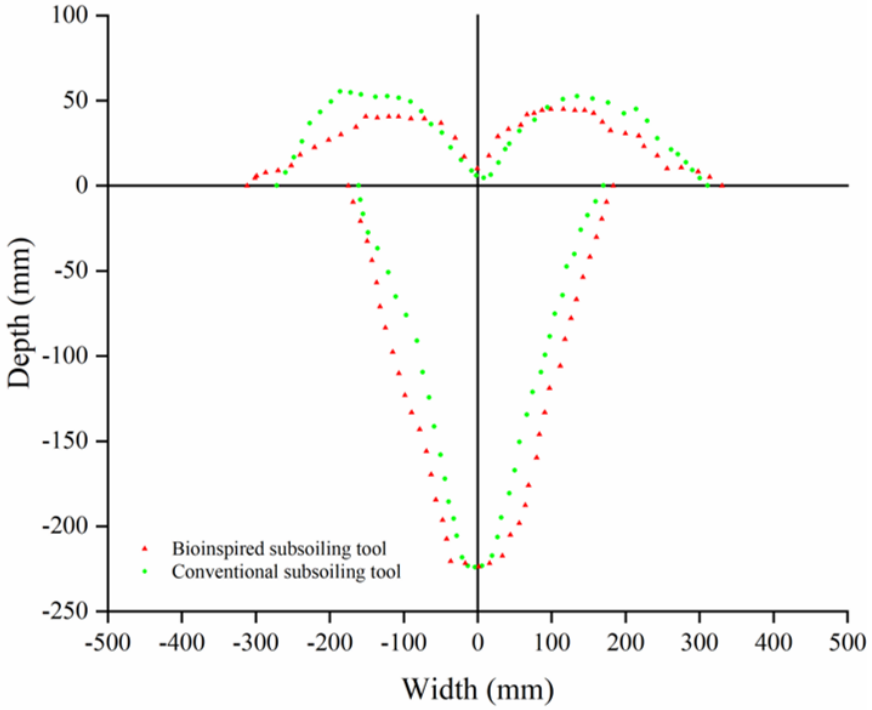

Figure 13. Comparison of soil disturbance profiles for bioinspired and conventional subsoiling tools.

Table 5. Soil disturbance parameters: bioinspired versus conventional subsoiling tools.

Parameter	Bioinspired	Conventional	Relative error (%)
Furrow cross-sectional area (mm^2)	54420	49743	8.6
Furrow width (mm)	363	337	7.2
Lateral soil throw (mm)	321	291	9.3
Ridge height (mm)	43	54	-25.6

3.4.3. Depth-Wise Distribution of Disturbed Soil Particle velocities within the designated velocity analysis zone were recorded 3 seconds after their creation, just before the subsoiler operation. The maximum observed velocity magnitude across all particles was 1.8 mm/s, which was established as the threshold for identifying disturbed soil particles. This approach is physically grounded: any particle velocity recorded before tool operation reflects only minor gravitational rearrangements after particle settling, and therefore represents the maximum ”background”

motion of the soil in its undisturbed state. By setting the disturbance threshold equal to this pre-tillage maximum velocity, the criterion ensures that only particles whose motion clearly exceeds the undisturbed-state envelope are classified as disturbed, providing a conservative and physically meaningful definition. This method is analogous to established practice in the DEM literature, where pre-tillage particle velocities or displacements are used as reference baselines for defining soil disturbance [7, 8]. Immediately after the subsoiling simulation run, particle velocities in the same analysis zone were recorded again. Particles with velocities exceeding 1.8 mm/s were considered to have been directly affected by the subsoiler operation. Using this criterion, the number of disturbed particles was determined within the analysis zone, which was divided into three depth intervals: 0–75 mm, 75–150 mm, and 150–225 mm, as illustrated in Figure 8. For each layer, the disturbed soil fraction was calculated as the percentage of disturbed particles in that layer relative to the total number of disturbed particles across the entire profile. The resulting data for both subsoiling tools are presented in Table 6. The results indicate that for both subsoiling tools, more than 50% of disturbed soil particles were located in the upper layer (0–75 mm). In the middle (75–150 mm) and lower (150–225 mm) layers, the bioinspired subsoiling tool achieved disturbance rates of 23.1% and 22.0%, respectively, substantially higher than those of the conventional subsoiling tool, which achieved 19.4% and 15.9%, respectively. This enhanced deep soil loosening is expected to improve the efficiency of rainwater and surface irrigation by facilitating the leaching and flushing of salts from the root zone into deeper soil layers, while also enhancing overall soil moisture retention [7].

The number of dislodged particles, defined as soil particles displaced from the original surface by the lifting action of the working tools, was assessed within the designated analysis zone for both subsoiling tool types. The bioinspired subsoiling tool dislodged 13,772 particles, while the conventional tool dislodged 12,819 particles. This represents a relative increase of approximately 6.9% for the bioinspired tool. While a lower number of dislodged particles typically indicates a smoother soil surface, this metric alone does not fully capture the post-tillage surface conditions. In this study, although the bioinspired tool produced more dislodged particles, it still resulted in a smoother soil surface than the conventional tool. This finding is supported by relevant evaluation parameters derived from the soil disturbance profiles (discussed in detail in Section 3.3.2). The analyses showed that the bioinspired tool reduced ridge height and increased lateral soil displacement, both of which indicate improved surface smoothing.

Table 6. Depth-wise distribution of disturbed soil for the bioinspired and conventional subsoiling.

Shank type **Dislodged Particles**	**Soil disturbance (%)**			**Total count of disturbed particles**
	Upper layer	**Middle layer**	**Lower layer**	
Bioinspired subsoiling tool 13772	54.9	23.1	22.0	19410
Conventional subsoiling tool 12819	63.7	19.4	15.9	18084

3.5. Effects of Rake Angle and Tillage Depth on the Bioinspired Subsoiler Performance

3.5.1. Influence of Rake Angle and Tillage Depth on DEM-Simulated Draft Force Draft force markedly increased with working depth, rising from 95 N at 50 mm to 881 N at 250 mm (Figure 14a). This trend is consistent with findings reported in the literature, although the functional form of the relationship differs across studies. Godwin and O'Dogherty [21] reported a linear relationship between draft force and working depth in their experimental study. In contrast, Li et al. [6] observed a power-law relationship between the two variables using DEM simulations. Similarly, draft force was also influenced by rake angle. At a tillage depth of 250 mm and a rake angle of 15°, the average draft force measured in the designated analysis zone was 820 N. Increasing the rake angle to 45° resulted in a corresponding increase in draft force, which reached 907 N (Figure 14b). This positive correlation between rake angle and draft force is consistent with findings reported in the literature. In a comprehensive review, Godwin

[22] concluded that rake angle significantly influences draft force across a range of 22.5° to 112.5°. Similarly, Li et al. [6] observed a positive correlation between rake angle and draft force when testing angles from 0° to 45°.

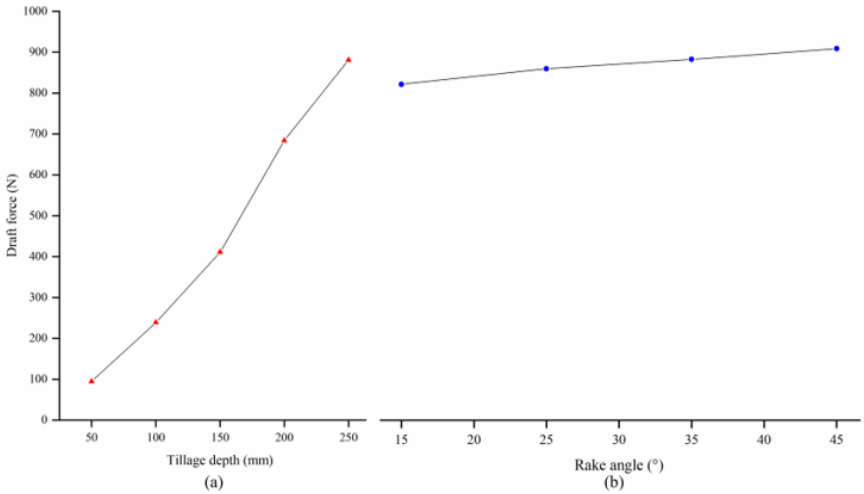

Figure 14. DEM-simulated draft force for the bioinspired subsoiler: (a) as a function of tillage depth (rake angle = 35°); (b) as a function of rake angle (tillage depth = 250 mm).

3.5.2. Influence of Rake Angle and Tillage Depth on DEM-Simulated Soil Bulk Density The initial soil bulk density before tillage was 1,504 kg·m^{-3} for all simulation runs. Following tillage at a depth of 50 mm, the bulk density within the analysis zone decreased to 1,490 kg·m^{-3}. Increasing the tillage depth from 50 mm to 250 mm resulted in a progressive further decrease in bulk density, reaching 1,396 kg·m^{-3} at 250 mm (Figure 15a). Similar trends were observed with increasing the cutting share rake angle. Following tillage at a rake angle of 15°, the bulk density within the designated analysis zone decreased to 1,454 kg·m^{-3}. Increasing the cutting share rake angle from 15° to 45° further decreased bulk density to 1,389 kg·m^{-3}. However, as illustrated in Figure 15b, the reduction rate was not uniform across this range; the most pronounced decrease occurred between 25° and 35°. This can be attributed to the enhanced vertical soil-lifting action within this interval, which promotes more intensive soil fracturing and consequently a greater reduction in bulk density. Overall, larger rake angles within the tested range produced lower bulk densities than smaller angles. Nevertheless, this beneficial effect must be balanced against the higher draft force and energy requirements associated with increased rake angles.

3.5.3. Influence of Rake Angle and Tillage Depth on DEM-Simulated Ridge Height The height of post-tillage ridges is influenced by the tool geometry and operating parameters [23]. The results demonstrated a strong positive correlation between tillage depth and ridge height, with the soil ridge profile increasing progressively as the bioinspired subsoiler's operating depth increased (Figure 16a). This trend can be attributed to the increased accumulation of soil particles ahead of the subsoiler at greater depths, which directly contributes to higher ridge formation. In contrast, increasing the cutting share rake angle from 15° to 45° reduced ridge height (Figure 16b). This decrease can be attributed to greater upward soil displacement at lower rake angles, which moves more material to the surface and consequently produces higher ridges.

3.5.4. Influence of Rake Angle and Tillage Depth on DEM-Simulated Lateral Soil Throw Lateral soil throw increased with tillage depth, rising from 218 mm at 50 mm to 334 mm at 250 mm (Figure 17a). This trend is consistent with previous findings indicating that deeper tillage depths result in greater lateral soil displacement [24]. As the tillage tool interacts with a larger volume of soil at greater depths, the cumulative effects of soil lifting and lateral displacement increase proportionally, resulting in the observed increase in lateral soil throw. In contrast,

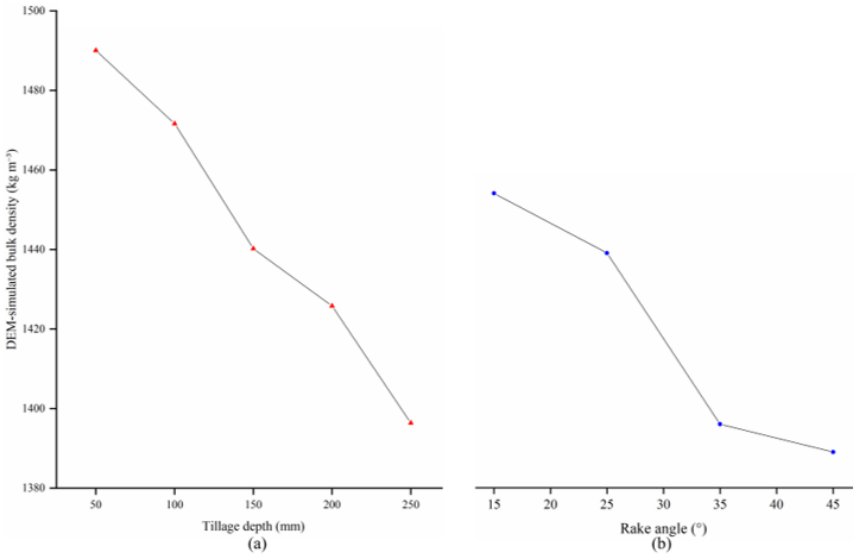

Figure 15. Soil bulk density following tillage with the bioinspired subsoiler: (a) as a function of tillage depth (rake angle = 35°); (b) as a function of rake angle (tillage depth = 250 mm).

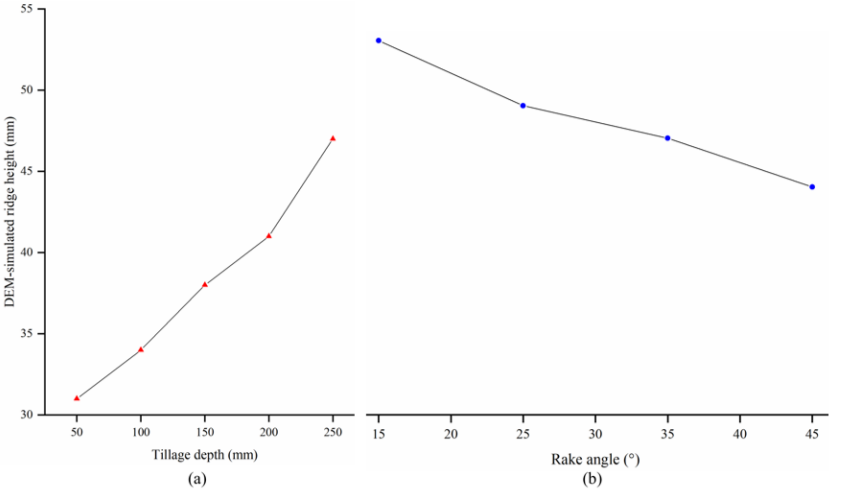

Figure 16. Post-tillage ridge height for the bioinspired subsoiler: (a) as a function of tillage depth (rake angle = 35°); (b) as a function of rake angle (tillage depth = 250 mm).

increasing the cutting share rake angle from 15° to 45° resulted in a notable reduction in lateral soil throw (Figure 17b). This finding is consistent with the research by Solhjou et al. [24], which showed that lower rake angles cause a gradual upheaval, moving soil from deeper layers upward and outward. It is important to note that this rake-angle parametric trend (lower angle → greater lateral throw) applies to systematic variation of the rake angle of a simple flat or chisel-type blade. The observation in Section 3.4.2 that the bioinspired tool (rake angle 35°, identical to the conventional tool) produces greater lateral throw than the conventional tool is not contradictory: in that comparison, both tools share the same nominal rake angle, and the increased lateral throw of the bioinspired shank arises from its

continuously curved surface geometry, which generates a distributed lateral force component along the full shank height. In contrast, the parametric study in this section isolates the effect of rake angle on the bioinspired shank alone, keeping geometry otherwise constant. The two effects, geometric curvature and rake angle, are therefore complementary rather than conflicting, and must be considered independently when interpreting lateral soil throw.

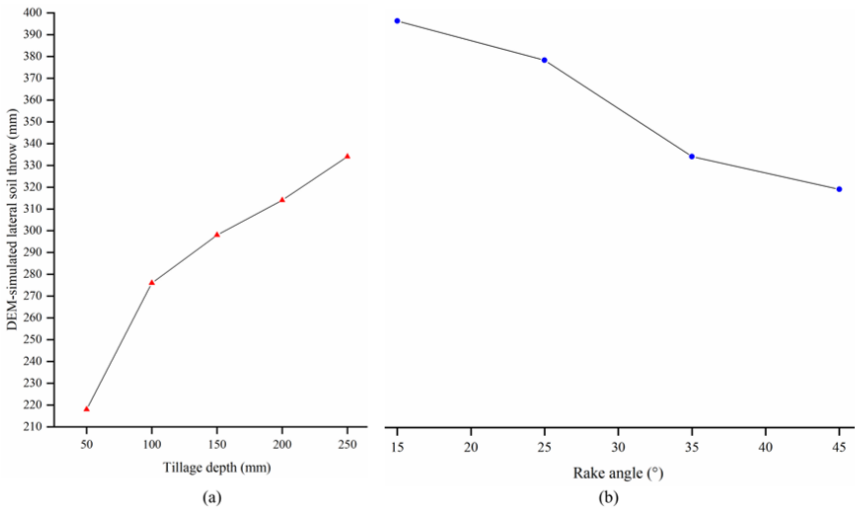

Figure 17. Post-tillage lateral soil throw for the bioinspired subsoiler: (a) as a function of tillage depth (rake angle = 35°); (b) as a function of rake angle (tillage depth = 250 mm).

3.5.5. Performance Evaluation The specific loosening resistance of the bioinspired subsoiler at various tillage depths is presented in Figure 18a. A positive correlation was observed between tillage depth and specific loosening resistance, with the value increasing at an accelerating rate at greater operating depths. This trend can be attributed to the greater soil strength and higher normal stresses encountered at greater depths, which directly contribute to increased cutting resistance. The proposed performance index was also utilized to assess the bioinspired subsoiler's performance at different rake angles (Figure 18b). Although the peak values at 35° and 45° were nearly identical, the 35° rake angle is preferred due to the higher draft force associated with steeper angles. Accordingly, a rake angle of 35° is recommended for the bear claw-inspired subsoiling shank when balancing draft force and soil disturbance.

Beyond the empirical measurements and DEM simulations presented in this study, the quantification of uncertainty and the assessment of model robustness can be further supported by statistical distribution theory. The characterization results based on generalized order statistics [27, 28, 29, 30, 31] provide a theoretical foundation for analyzing the stochastic nature of draft force fluctuations and soil disturbance variability. Moreover, flexible parametric distributions [26, 32] offer alternative specifications for residual error analysis, particularly in evaluating the sensitivity of the DEM predictions to input parameter variations. These theoretical tools complement the experimental–numerical framework adopted herein, especially in assessing the reliability of the observed performance improvements under different operational conditions.

4. Conclusions

Inspired by the exceptional digging abilities of brown bears, this study developed a subsoiling shank designed to improve tillage efficiency and soil disturbance quality. The discrete element method (DEM) input parameters for characterizing the adhesive loam soil properties in the Yellow River Delta (YRD), China, were successfully

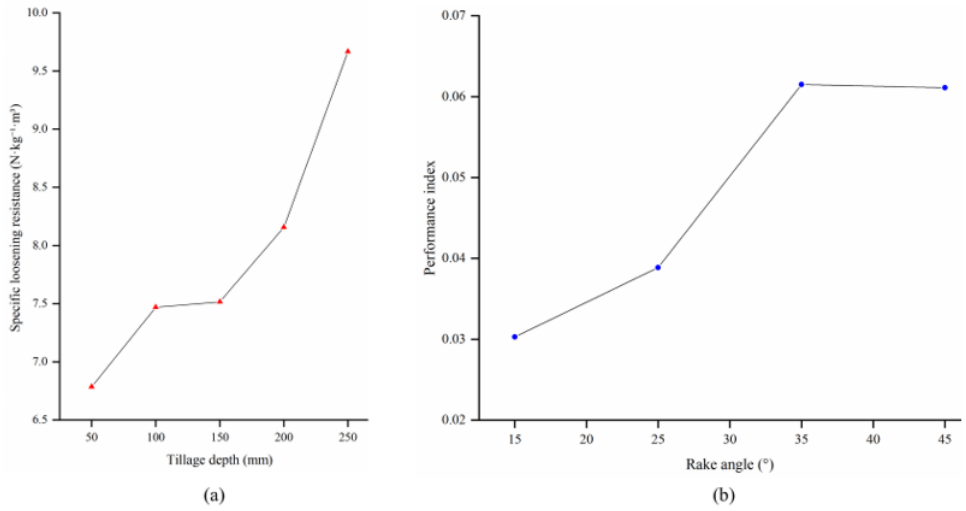

Figure 18. Performance evaluation of the bioinspired subsoiler: (a) specific loosening resistance for different tillage depths (rake angle = 35°); (b) performance indices for different rake angles (tillage depth = 250 mm).

identified and validated. Calibration was based on three key criteria: interparticle friction, determined through the angle of repose test; soil-tool adhesion, quantified via the direct shear test; and contact model input parameters, calibrated by aligning simulated particle packing density with experimentally measured soil wet bulk density. The calibrated DEM model demonstrated strong predictive capability for draft force (10% relative error) and acceptable predictive capability for soil disturbance parameters (relative errors ranging from 16.6% to 32.8%).

Using the validated DEM model, a comparative analysis was performed between the bio-inspired subsoiling tool and a traditional subsoiling tool. Compared with a conventional straight shank, the bioinspired subsoiler achieved a 6.1% reduction in draft force, an 8.6% increase in furrow cross-sectional area, and a 25.6% reduction in ridge height, reflecting enhanced soil loosening and improved surface smoothing. This performance improvement extended to deeper soil layers: in the middle (75–150 mm) and lower (150–225 mm) layers, the bioinspired tool achieved disturbance rates of 23.1% and 22.0%, respectively, substantially higher than those of the conventional tool (19.4% and 15.9%, respectively). Such enhanced deep loosening is expected to improve rainwater and irrigation usage efficiency by facilitating salt leaching from the root zone into deeper soil layers while enhancing overall soil moisture retention. Parametric analysis revealed that increasing tillage depth from 50 mm to 250 mm increased draft force, ridge height, and lateral soil throw. Conversely, increasing the rake angle from 15° to 45° reduced ridge height and lateral soil throw but increased draft force. Based on these findings, a rake angle of 35° is recommended for optimal performance, balancing draft force reduction with favorable soil disturbance characteristics. Overall, the bear claw-inspired subsoiling shank offers a promising design solution for improving tillage efficiency and soil disturbance quality. Furthermore, the validated DEM model provides a reliable tool for optimizing soil-engaging components in conservation agriculture.

Author Contributions

Conceptualization, A.S. and R.M.K.; methodology, A.S. and F.M.S.; software, A.M.H.; validation, X.Z.; formal analysis, R.M.; writing—original draft preparation, A.M.H.; writing—review and editing, R.M.K., S.Y., F.M.S., and F.A.A.; supervision, A.S.; project administration, A.S.; funding acquisition, S.Y. and F.A.A; Language editing and manuscript revision were performed by S.Y.

Data Availability Statement

The original contributions presented in this study are included in the article. Further inquiries can be directed to the corresponding authors.

Conflicts of Interest

The authors declare no conflicts of interest.

REFERENCES

1. C.G. Henry, G.M. Sarzi Sartori, J.P. Gaspar, E. Marchesan, S.M. Hirsh, A.P. Horton, L. Espinoza, and H. James, *Deep tillage and gypsum amendments on fully, deficit irrigated, and dryland soybean*, Agron. J., vol. 110, pp. 737–748, 2018.
2. Z. Ding, A.M. Kheir, O.A. Ali, E.M. Hafez, E.A. ElShamey, Z. Zhou, B. Wang, X.E. Lin, Y. Ge, and A.E. Fahmy, *A vermicompost and deep tillage system to improve saline-sodic soil quality and wheat productivity*, J. Environ. Manag., vol. 277, p. 111388, 2021.
3. X. Wang, R. Du, L. Geng, H. Zhou, and J. Ji, *Performance evaluation of a cicada-inspired subsoiling tool using DEM simulations*, Biomimetics, vol. 9, p. 25, 2024.
4. J. Sun, Y. Wang, Y. Ma, J. Tong, and Z. Zhang, *DEM simulation of bionic subsoilers (tillage depth ¿ 40 cm) with drag reduction and lower soil disturbance characteristics*, Adv. Eng. Softw., vol. 119, pp. 30–37, 2018.
5. M. Barzegar, S. Hashemi, H. Nazokdast, and R. Karimi, *Evaluating the draft force and soil-tool adhesion of a UHMW-PE coated furrower*, Soil Tillage Res., vol. 163, pp. 160–167, 2016.
6. B. Li, Y. Chen, and J. Chen, *Modeling of soil–claw interaction using the discrete element method (DEM)*, Soil Tillage Res., vol. 158, pp. 177–185, 2016.
7. C. Hang, X. Gao, M. Yuan, Y. Huang, and R. Zhu, *Discrete element simulations and experiments of soil disturbance as affected by the tine spacing of subsoiler*, Biosyst. Eng., vol. 168, pp. 73–82, 2018.
8. K.A. Aikins, M. Ucgul, J.B. Barr, T.A. Jensen, D.L. Antille, and J.M.A. Desbiolles, *Determination of discrete element model parameters for a cohesive soil and validation through narrow point opener performance analysis*, Soil Tillage Res., vol. 213, p. 105123, 2021.
9. M. Ucgul and C. Saunders, *Simulation of tillage forces and furrow profile during soil-mouldboard plough interaction using discrete element modelling*, Biosyst. Eng., vol. 190, pp. 58–70, 2020.
10. E. McKyes and J. Maswaure, *Effect of design parameters of flat tillage tools on loosening of a clay soil*, Soil Tillage Res., vol. 43, pp. 195–204, 1997.
11. J.B. Barr, M. Ucgul, J.M.A. Desbiolles, and J.M. Fielke, *Simulating the effect of rake angle on narrow opener performance with the discrete element method*, Biosyst. Eng., vol. 171, pp. 1–15, 2018.
12. S.H. Hoseinian, A. Hemmat, A. Esehaghbeygi, G. Shahgoli, and A. Baghbanan, *Development of a dual sideway-share subsurface tillage implement: Part 2. Effect of tool geometry on tillage forces and soil disturbance characteristics*, Soil Tillage Res., vol. 215, p. 105200, 2022.
13. A. El Salem, S. Shang, D. Wang, G. Zhang, H. Wang, M.A. Abdeen, and T.A. Shehabeldeen, *Developing an adequate DEM model to simulate soil-tool interactions under sticky soil conditions*, Soil Tillage Res., vol. 256, p. 106893, 2026.
14. M. Ucgul, J.M. Fielke, and C. Saunders, *Three-dimensional discrete element modelling (DEM) of tillage: Accounting for soil cohesion and adhesion*, Biosyst. Eng., vol. 129, pp. 298–306, 2015.
15. S. Mudarisov, I. Farkhutdinov, R. Khamaletdinov, E. Khasanov, and A. Mukhametdinov, *Evaluation of the significance of the contact model particle parameters in the modelling of wet soils by the discrete element method*, Soil Tillage Res., vol. 215, p. 105228, 2022.
16. M. Ucgul, J.M. Fielke, and C. Saunders, *Three-dimensional discrete element modelling of tillage: Determination of a suitable contact model and parameters for a cohesionless soil*, Biosyst. Eng., vol. 121, pp. 105–117, 2014.
17. S. Murray, *Modelling of soil-tool interactions using the discrete element method (DEM)*, Master's Thesis, University of Manitoba, Winnipeg, MB, Canada, 2016.
18. B. Wu, R. Zhang, P. Hou, J. Tong, D. Zhou, H. Yu, Q. Zhang, J. Zhang, and Y. Xin, *Bionic nonsmooth drag reduction mathematical model construction and subsoiling verification*, Appl. Bionics Biomech., vol. 2021, p. 5113453, 2021.
19. Z. Xu, H. Qi, L. Wang, S. Wang, X. Liu, and Y. Ma, *DEM study and field experiments on coupling bionic subsoilers*, Biomimetics, vol. 10, p. 306, 2025.
20. F. Garibaldi-Márquez, E. Martínez-Reyes, C. Morales-Morales, L. Ramos-Cantú, M. Castro-Bello, and A. González-Lorence, *Subsoiler tool with bio-inspired attack edge for reducing draft force during soil tillage*, AgriEngineering, vol. 6, pp. 2678–2693, 2024.
21. R.J. Godwin and M.J. O'Dogherty, *Integrated soil tillage force prediction models*, J. Terramech., vol. 44, pp. 3–14, 2007.
22. R.J. Godwin, *A review of the effect of implement geometry on soil failure and implement forces*, Soil Tillage Res., vol. 97, pp. 331–340, 2007.
23. T. Wang, Z. Yu, F. Meng, Y. Chen, and R. Wang, *Simulation analysis and experiment for operation performance of interval subsoiler based on discrete element method*, Trans. Chin. Soc. Agric. Mach., vol. 56, no. 4, pp. 98–106, 2025.
24. A. Solhjou, J.M. Fielke, and J.M.A. Desbiolles, *Soil translocation by narrow openers with various rake angles*, Biosyst. Eng., vol. 112, pp. 65–73, 2012.

25. H.M. Hanna, S.J. Marley, D.C. Erbach, and S.W. Melvin, *Change in soil microtopography by tillage with a sweep*, Trans. ASAE, vol. 36, pp. 301–307, 1993.
26. K.A.E. Gad, F.A. Atia, M. Moussa, H.M. Hamouda, and M.F. Abouelenein, *The Fractional Exponential Distribution: A Gamma Subfamily from Conformable Calculus*, Results in Engineering, p. 111224, 2026.
27. A.A. Ali, M. Ali, K.A. Gad, and S.M. Assar, *Some Characterizations Based on Generalized Order Statistics from Power Inverted Topp–Leone Distribution*, Adv. Nonlinear Var. Inequal., vol. 28, no. 6s, pp. 349–365, 2025.
28. K.A.E. Gad, I.B. Abdul-Moniem, and S.M. Assar, *Some Characterizations Based on Generalized Order Statistics from Weibull-Weibull Distribution*, Egypt. Stat. J., vol. 67, no. 2, pp. 1–16, 2023.
29. A.A. Abdul-Rahman, I.B. Abdul-Moniem, K.A.E. Gad, and S.M. Assar, *Some Characterizations Based on GOS from Weibull-Weibull Distribution (Part II)*, Egypt. Stat. J., vol. 67, no. 2, 2023.
30. I.B. Abdul-Moniem, K.A.E. Gad, and S.M. Assar, *Characterization of Phani Distribution Based on Generalized Order Statistics*, Sohag J. Sci., vol. 9, no. 1, pp. 32–39, 2024.
31. A.A. Abdul-Rahman, I.B. Abdul-Moniem, K.A.E. Gad, and S.M. Assar, *Some Characterizations Based on Generalized Order Statistics from Weibull-Family of Life Distributions*, Proc. 56th Annu. Int. Conf. Data Sci., 2024.
32. A.S. Hassan, I.B. Abdul-Moniem, and K.A.E. Gad, *A Generalized Transmuted Moment Exponential Distribution: Properties and Application*, Acad. J. Appl. Math. Sci., vol. 6, no. 5, pp. 41–52, 2020.